EGYPTIAN JOURNAL OF BOTANY (EJBO)

Print ISSN: 0375-9237
Online ISSN: 2357-0350

Mycosynthesis of some nanocomposite films using *Aspergillus ochraceus* NSRN22 for the preservation of postharvest lemons

Nesren M. El-Basiouny, Soliman M. Abd El-latif, Neveen M. Khalil, Mohamed N. Abd El-Ghany

PUBLISHED BY
THE EGYPTIAN
BOTANICAL SOCIETY

Mycosynthesis of some nanocomposite films using *Aspergillus ochraceus* NSRN22 for the preservation of postharvest lemons

Nesren M. El-Basiouny[1], Soliman M. Abd El-latif[2], Neveen M. Khalil[1], Mohamed N. Abd El-Ghany[1]

[1]Botany and Microbiology Department, Faculty of Science, Cairo University, Giza 12613, Egypt
[2]Chemistry Department, Faculty of Science, Cairo University, Giza 12613, Egypt

The isolated *Aspergillus ochraceus* was utilized to create silver and selenium nanoparticles (AgNPs and SeNPs) using its cell-free filtration (CFF). Particle sizes for SeNPs ranged from 32.3 to 50.7 nm, whereas those for AgNPs ranged from 6.41 to 11 nm. The biosynthesized NPs were mixed with either sodium alginate (SA) or chitosan (CS) to create a novel food packaging film. Using scanning electron microscopy (SEM), ultraviolet-visible spectroscopy (UV-Vis), and Fourier transform infrared spectroscopy (FTIR), the produced films were functionally and morphologically characterized. Composite films were tested for biodegradability, cytotoxicity, water vapor transmission rate, mechanical strength, solubility, and antifungal activity. When comparing SA/NPs with CS/NPs, the latter had superior biological, mechanical, antifungal and antioxidant properties. In the case of nanocomposite films containing CS/AgNPs, CS/SeNPs, SA/AgNPs, and SA/SeNPs, respectively, the tensile strength of CS (0.58 MPa) or SA (2.42 MPa) increased to 4.15 MPa, 4.16 MPa, 3.07 MPa and 2.48 MPa. However, for CS/AgNPs, CS/SeNPs, SA/AgNPs, and SA/SeNPs, respectively, the water vapor pressures decreased from 2021.57 g/m^2.day for CS and 2132.59 g/m^2.day for SA to 1559.94, 1518.93, 1945.24 and 1775.96 g/m^2.day. For CS/AgNPs, CS/SeNPs, SA/AgNPs, SA/SeNPs, CS, and SA, the corresponding statistical minimum inhibitory concentrations were 1020, 1040, 1080, 1025, 1160, and 1160 µg/ 5 mL. When formed films are compared to films made of plastic, the nanocomposite films with NPs significantly reduce *Penicillium citrinum* contamination. Specifically, the produced CS/SeNPs films show a lot of promise as nontoxic antimicrobial active packaging components that could prolong the freshness of fruits and other foods.

Keywords: SeNPs, AgNPs, Chitosan, Sodium Alginate, Biopolymer, Mycosynthesis, Nanocomposite, Food Packaging, Postharvest fruit preservation

ARTICLE HISTORY
Submitted: December 05, 2024
Accepted: January 02, 2025

CORRESPONDENCE TO
Mohamed N. Abd El-Ghany,
Botany and Microbiology Department,
Faculty of Science, Cairo University,
Giza 12613, Egypt
Email: mabdelghany@sci.cu.edu.eg
DOI: 10.21608/ejbo.2025.342066.3110

EDITED BY: A. Saleh

INTRODUCTION

The food industry has been looking into biopolymer food packaging films with natural ingredients for some time. Food packaging has multiple purposes: preventing microbiological spoilage, making food safe, making it last longer, and reducing environmental impact (Alizadeh-Sani et al., 2021). In contrast to synthetic plastics made from petroleum, which are not biodegraded, biocompatible packaging materials and biopolymers are currently quite popular (Bagheri et al., 2019). Biodegradable polymers, which are non-toxic and have ecologically friendly characteristics, and other naturally occurring biologically active substances that enhance food quality, have been utilized because of increasing population, environmental threats, and human health issues. The antimicrobial, antifungal, and antioxidant characteristics of nanocomposite films enhanced with natural essential oils/or extracts make them ideal for use in food packaging (Alizadeh-Sani et al., 2019).

A natural and widespread biopolymer that comes from chitin; chitosan has gained attention as a potential material for food packaging because of its distinctive features. In addition to reducing the need for traditional polymers, the use of chitosan in food packaging offers a fantastic answer to the environmental problems caused by the seafood industry, since chitin is derived from seafood waste. The fact that it is edible, biodegradable, and possesses antimicrobial properties further adds to its attraction as a safer and more environmentally friendly substitute for synthetic polymers (Flórez et al., 2022). Its compatibility with other materials enables the fabrication of new packaging solutions and its good mechanical and barrier capabilities against gases like O_2 and CO_2 make it suited for various types of packaging. So, chitosan-based food packaging could form a solution to two problems: less plastic waste and better food quality and safety (Devi et al., 2024).

Both the European Food Safety Authority and the US Food and Drug Administration have recognized sodium alginate as safe for human health; it is a biodegradable and non-toxic polymer found in the cell walls of brown seaweeds in the *Phaeophyceae* class (Tran et al., 2023). Various antimicrobial compounds are added to packaging using alginates as a substrate. This helps to protect food from microorganisms. Biotechnology and food industries have found many uses for this biopolymer due to its abundance, low cost, biocompatibility, and environmental friendliness. Some of these uses include thickening and gelling agents, colloidal stabilizers, and non-toxic food additives (Carneiro-da-Cunha et al., 2010).

Incorporating active additives like plant extracts and/or nanoparticles into films and edible coatings made of sodium alginate or chitosan presents numerous possibilities for producing novel food packaging. Zinc, iron, gold, silver, selenium, and titanium dioxide are antimicrobial NPs that are applied in active packaging to prevent microbial growth, improve product quality, and extend the shelf life of food products.

In humans, selenium (Se) plays a crucial role in a variety of metabolic activities, including DNA synthesis, antioxidant defense, infection protection, and selenoprotein and selenoenzyme composition (Rayman, 2012). Nanoparticles of selenium, or SeNPs, are created when basic selenium undergoes a state of no oxidation. SeNPs are absorbed by the human body at a significantly higher rate compared to other types of Se. SeNPs have been found to have less toxicity in studies compared to oxidized Se^{2+}, Se^{4+}, Se^{6+}, and Se^{2-} (Wang et al., 2007). SeNPs are bio-available and exhibit anti-inflammatory, anti-cancer, and anti-diabetic characteristics (El Refai et al., 2024). As a result, SeNPs have been the subject of much interest because of their potential medical and food-related uses.

Due to their unique physicochemical, optical, catalytic, antimicrobial, and thermally stable properties, silver nanoparticles (AgNPs) have found extensive use in a variety of industries, including electrical, medical, pharmaceutical, food, and food packaging (Shankar et al., 2015). For industries such as food packaging, biomedicine, and pharmaceuticals, AgNPs' antibacterial activity is a crucial property. In general, it is known that the synthesis processes, in addition to the type of silver, size, and shape, determine the antibacterial activity of AgNPs.

The synthesis of NPs has made use of several different approaches. Biobased synthesis, often known as "green synthesis," makes use of microbes, plants, and yeasts. Fungi are the best microbes to use because they multiply quickly, have useful bio-properties, and have readily available, simple structures. On top of that, these creatures produce the greatest number of biomolecules, which trigger the production of NPs. Numerous studies have focused on the synthesis of metallic and oxide NPs and have shown that fungi may be able to produce a variety of NPs via both intracellular and extracellular pathways (Shaheen et al., 2021).

This study was designed to examine the antifungal activities of nanocomposite films synthesized using a green method, which would be based on nanoparticles and either chitosan or alginate. Further, there were investigations of thermal, mechanical, and barrier properties concerning water, as well as the antimicrobial effectiveness of the produced films and the effects of different types of nanoparticles against the fungus *Penicillium citrinum*. Water vapor permeability (WVP), film thickness, water solubility, and other experiments were performed to fully evaluate these films. Furthermore, the quality of lemons covered by these films was examined.

MATERIALS AND METHODS

Fungal strain, media, and culture conditions

Soil dilution plates, as described in Johnson (1959), were used to obtain the tested fungus from the Iron and Steel Factory in Helwan, Egypt. On a Czapek-Dox agar (CZA) medium, soil samples were used as an inoculum. To ensure that only pure fungal colonies were obtained, the streak plate approach was used. The fungus was grown on slants with CZA at 28 °C for 4 days. The spores of the fungus were preserved at 4 °C in a sterile spore suspension buffer that included 0.9% (w/v) NaCl and 1% (v/v) Tween 80 (Abd El-Ghany et al., 2023a).

Molecular identification of the fungal isolate

The identification of the fungus was confirmed using nuclear ribosomal DNA internal transcribed spacer (ITS) sequencing. We used the primer ITS (CTTGGTCATTTAGAGGAAGTAA) to amplify the 18S ribosomal RNA gene, the internal transcribed spacer 1, 5.8S ribosomal RNA gene internal transcribed spacer 2, and 28S ribosomal RNA gene. The GATC Company (Germany) was tasked with sequencing the amplified product using their polymerase chain reaction product. An entry was made in the GenBank database at the National Center for Biotechnology Information (NCBI). An accession number and a strain identifier were given to the isolate.

Synthesis and detection of the NPs

The fungus stock spore suspensions were added into 100 mL of MGYP medium (0.3% malt extract, 1% glucose, 0.3% yeast extract, and 0.5% peptone; pH 6.8) in 250 mL cotton-plugged Erlenmeyer flasks, as per the instructions given in Khalil et al. (2019). For one day at 28 °C, the flasks were shaken in an incubator at 150 rpm. The inoculum (10% v/v) was prepared using the same medium and culture conditions as the starter culture; the only difference being a three-day incubation period. Finally, to

remove any residual culture material, the fungal mycelium was centrifuged at 5000 rpm for 15 min at 4 °C. The contents of the biomass, including intracellular enzymes, were discharged into a watery solution after autolysis. The result was achieved by adding 10 g of fresh biomass to 100 mL of sterile deionized water and stirring gently for 15 min at 28 °C. The CFF was obtained by separating the cells from the flask's contents using Whatman filter paper no. 1. Fifty mL of CFF and 10 mL of 10 mM $AgNO_3$ were mixed and then incubated at 28 °C with 150 rpm of shaking in the absence of light to produce AgNPs (Abd El-Ghany et al., 2023b).

According to Salem et al. (2021), 100 mL of CFF was combined with 0.026 g of sodium selenite, and the pH was brought to 6.5 using ascorbic acid to biosynthesize the SeNPs. The reaction mixture was incubated at 30 °C and agitated at 120 rpm for 24 hours. Upon completion of the NPs production process, the mixture of AgNPs or SeNPs was centrifuged at 10000 rpm and 4 °C for 15 min. The centrifuged NPs were cleaned and made purer by rinsing them in distilled water and acetone many times. After the NPs were dried, their size, shape, charge, and morphology were studied.

Characterization of the NPs

UV–Vis Spectrum Analysis: A UV-Vis spectrophotometer (Perkin-Elmer Hitachi 2000 model) was used to measure spectra within the 360-600 nm range. This was done as part of the physiochemical identification processes that aimed at characterizing the materials.

Transmission Electron Microscopy (TEM): The nanoparticles' size, shape, and dispersion were evaluated using TEM (JEOL-2100).

Dynamic Light Scattering (DLS): Using the dynamic light scattering (DLS) method, we were able to measure the particle size of the prepared samples. While the solution was kept at room temperature, the dispersion of the nanoparticles was examined using the PSSNICOMP Zeta Potential/Particle Sizer 380ZLS (PSS-NICOMP, Santa Barbara, CA, USA). The nanoparticles' zeta potential was measured using a Zetasizer Nano ZS ZEN3600 produced by Malvern Instruments Ltd. of Worcestershire, UK. Charges and stability of NPs were determined by measuring their Zeta potential.

FT-IR Spectroscopy: The main functional groups that had formed on the surfaces of the nanoparticles were estimated to be using the FTIR spectrometer JASCO, FT/IR-6100. A 4 cm^{-1} resolution was used to scan the spectra from 400 to 4000 cm^{-1}.

XRD Analysis: Crystallinity, crystallite size, and crystal lattice were determined using the XRD-6000 lists, Shimadzu equipment, SSI, Japan. The intensity of the dispersed X-rays was measured using diffraction angle 2.

Antifungal activity of synthesized NPs

The postharvest fruit-infecting fungus *Penicillium citrinum* was isolated, purified, and identified from infected lemons. It was then tested for the effectiveness of AgNPs and SeNPs in suppressing spore germination. The minimum inhibitory concentration (MIC) was determined. Each microtiter plate was inoculated with 50 µL of spore suspension after being mixed with 100 µL of Czapek-Dox media and different quantities of AgNPs and SeNPs. Using itraconazole, as positive control, and double-distilled water, as a negative control, they were components of the experimental design. The spores germinated on the plate after 16 hours of incubation at 30 °C. To be classified as germinated, the germ tube's length must be double that of the spore's size. (Griffin, 1994). The MIC refers to the concentration of AgNPs and SeNPs that were required to completely block spore germination.

Preparation of nanocomposite films

Alginate nanocomposite film: When the solution containing 1 g of sodium alginate (w/w %) in 100 mL of distilled water had cooled to 70 °C, it was mixed with 0.05 g of nanoparticles. The mixture also contained 1 mL of glycerol and 1 mL of Tween 80 (an emulsifier and surfactant). The mixture was cast into equally sized petri dishes after 2 hours of mixing and let to dry at room temperature for 24 hours.

Chitosan nanocomposite film: One gram of chitosan will be mixed with 100 mL of a 1% acetic acid solution, heated to 70 °C, cooled, and then treated with 1 mL of glycerol and Tween 80, respectively. A weight of 0.05 g of nanoparticles was added and the final mixture was well mixed for a duration of two hours prior to being transferred to petri dishes of consistent size.

Characterization of nanocomposite films

Nanocomposite films were characterized using a UV-Vis spectrophotometer, Fourier transform infrared (FT-IR) spectroscopy, and XRD.

SEM with EDX: Using an Energy Dispersive X-ray Analyses (EDX) Unit in conjunction with a scanning

electron microscope (SEM, Quanta FEG 250, FEI, Republic of Czech) allowed for a morphological analysis of the atomic distribution and percentages in the films.

Mechanical properties: The films' mechanical characteristics were measured using a texture analyzer (CT3, Brookfield, USA) that applied a modified version of the standard method ASTM D882/12. The film was measured for thickness after being cut into 1-by-6-centimeter strips. For calculating the tensile strength (TS) and the elongation at break (EAB), the following formulae were used:

$$\text{TS (Mpa)} = \frac{F}{h \times d}$$

$$\text{EAB (\%)} = \frac{L - L^{\circ}}{L^{\circ}} \times 100$$

Where F (N) was the maximum tension at film break, d (mm) was the film thickness, h (mm) was the width of the film; L (mm) was the length of the film after stretching, and L^0 (mm) was the initial length of the film.

Thermal analysis: The temperature was scanned from 10 to 600 °C at a rate of 10 °C/min. The TGA curve was used to determine the percentage of weight loss and the maximum decomposition temperature of the films.

Moisture content (MC) and water solubility (WS): After weighing the film strips (20 mm x 20 mm) (W_0), they were subjected to a vacuum drying oven set at 105 °C for three hours, following which they were reweighed (W_1). After the film had been dried, it was combined with 30 mL of distilled water and left to sit at room temperature for 48 hours to rehydrate. After collecting the residual film, it was dried at 50 °C for 24 hours and then measured as W_2. (Hu et al., 2021). To find the MC and WS of the film, these formulae were used:

$$\text{MC (\%)} = \frac{W^{\circ} - W1}{W^{\circ}} \times 100$$

$$\text{WS (\%)} = \frac{W1 - W2}{W1} \times 100$$

Where W_0 (g) was the initial mass of the film sample, W_1 (g) was the weight of the dry initial film sample and W_2 (g) was the final dry mass of the film sample.

Water vapor permeability (WVP): The films' water vapor permeability (WVP) was calculated using a modified version of the American Society for Testing and Materials (ASTM) standard (Xu et al., 2019). The following formula was used to determine the WVP:

$$WVP\ \left(\frac{g.m}{h.m^2.Pa}\right) = \frac{\Delta m\ X\ d}{t \times A \times \Delta p}$$

Where △m (g) was the weight gain, d (m) was the thickness of the film sample, t (h) was the time for the weight gain of the test cup, A (m2) was the permeation area of the film sample and △p (Pa) was the water vapor pressure difference between both sides of the film sample.

Water contact angle (WCA): The hydrophilicity or hydrophobicity of the film's surface was qualified by measuring its water contact angle (WCA). A sessile drop test was performed in air using a drop shape analyzer (DSA25S, KRUSS, Hamburg, Germany) to evaluate the contact angle.

Antioxidant effect of the films

The films' capacity to scavenge free radicals was evaluated by measuring their hydrogen-donating or radical-scavenging capabilities using the stable free radical DPPH. Using a method outlined in Ansari et al. (2013), the films' capacity to neutralize DPPH radicals was assessed. The final volume was 1.5 mL, which was achieved by mixing a 1 mM DPPH solution in ethanol with a 1 mg/mL extract solution in ethanol. At 517 nm, the findings were compared to those obtained with a 3 mL ethanol blank solution and a 3 mL DPPH control optical density (ODT). A total of three tests were performed. Using the following equation, we were able to calculate the percentage of the free radical DPPH that was inhibited:

$$\text{DPPH scavenged (\%)} = \frac{(A\ con - A\ test)}{A\ con} \times 100$$

Where (A con) is the absorbance of the control reaction and (A test) is the absorbance in the presence of the sample of the films.

Cytotoxicity evaluation

We utilized the baby hamster kidney cells (BHK), which are normal cells from the Faculty of Nanotechnology for Postgraduate Studies at Cairo University. Two groups of cells were prepared for the experiment: one group acted as a control, and the other group was exposed to varying concentrations of the films (0.25, 0.5, 1, and 2 mg/mL). After 24 hours, 10 µL of the MTT reagent (with a concentration of 0.5 mg/mL) was added to each well. The microplate was given a 4-hour incubation period. Each well was filled with 100 µL of the solubilization solution. After the purple formazan crystals had dissolved completely, the absorbance of the samples was determined using an ELISA reader for microplates. The optimal wavelength for measuring the absorbance of

formazan products is 570 nm. Using the following formula, the percentage of cells that were considered viable was quantified:

The cell viability (%) = [ODS/ ODC] × 100.

The sample's mean optical density is denoted as ODS, while the control's mean optical density is represented by ODC .

Biodegradability in soil

The film's dry samples were immersed in a 10 cm deep pot of soil for a week or two to find out how biodegradable it was. After putting the pot in the lab, watering it regularly was ensured to maintain the soil moist. If there was an excess of water, it could simply drain out through a hole in the pot's base. Following a two-week interval, the films were removed, cleaned, and allowed air dry at 50 °C. The degradation value of the films was calculated using the following equation:

$$\text{Degradation (\%)} = \frac{(W0 - Wf)}{W0} \times 100$$

The weight of the sample after testing is denoted by W_f, while the weight of the dry film before testing is W_0.

Antifungal activity of nanocomposite films

In this experiment, the Czapek-Dox medium was used to grow the *Penicillium citrinum* fungus. Five mL of the mentioned medium was placed into each falcon vial for culture. Different concentrations of the films were tested, including 62.5, 125, 250, and 500 µg/5 mL. To create inocula, spores were extracted from 7-day-old slants of the tested fungus and mixed with sterilized distilled water that included 0.1% (v/v) Tween-80. For every falcon, 100 µL of spore solution was added. The falcons were kept in a shaking incubator at 30 °C and 160 rpm for 7 days. The culture filtrate was filtered using Whatman filter paper No. 1 to extract the mycelium. After making replications, the mycelial mat was oven-dried at 80 °C until it achieved a constant weight, and then the dry weight was quantified as mg/mL of growing culture.

Packaging efficiency of nanocomposite films

The weight loss of lemons was examined to find out how to make them last longer in the fridge (Kanikireddy et al., 2019). Fresh lemons were procured from the market and then rinsed in water that had been double-distilled. After washing, the lemons were divided into two groups. One set, which acted as a control, was created without the use of nanocomposites, whereas the other set had them applied. After submerging the lemons in a beaker with the prepared film solution for 5 minutes, it was removed and allowed to dry. The weight loss of the lemons was monitored for 20 days using these films, which were maintained at 5 °C. To find out how much weight the lemons lost, the following equation was used:

$$\text{Weight loss } (W_L) = \frac{Wi - Wt}{Wi} \times 100$$

Where W_t is the weight of the tomatoes at time t, and W_i is their initial weight.

Statistical analysis

The mean of three independent tests was represented in each experiment. The SPSS program was used to conduct regression analysis to determine the standard deviation (SD), standard error (SE), least significant difference (LSD), and regression analysis.

RESULTS AND DISCUSSION

Isolation of fungal strain

For this research, *Aspergillus ochraceus* was first isolated and then purified. Internal transcribed spacer (ITS) sequencing nuclear ribosomal DNA confirmed the isolates' identities. A hybrid approach was used to sequence the PCR products, combining the more traditional Sanger method with the more recent 454 method. Successfully deposition of the obtained nucleotide sequence at the NCBI GenBank was conducted with the help of a strain identifier. As a result, the accession number PQ590684 was assigned to the isolate *Aspergillus ochraceus* NSRN22. *Aspergillus ochraceus* NSRN22 was used as a cell manufacturer to produce AgNPs and SeNPs.

Biosynthesis and detection of the NPs

The NPs were made using the Cell Free Filtrate (CFF) that was extracted from the autolyzed biomass, ensuring that no mycelial components were present. In the CFF, there are proteins and enzymes. The fungus *Aspergillus ochraceus* NSRN22 releases metabolites that reduce the concentration of silver ions to nanoparticles (AgNPs) and selenium ions to nanoparticles (SeNPs). The successful synthesis of SeNPs and AgNPs was indicated by the appearance of ruby red or brown colors after combining the biomass filtrate of *Aspergillus ochraceus* NSRN22 with sodium selenite or an $AgNO_3$ solution, respectively. The reaction was then terminated. After that, the colloidal solution of the two NPs was dried in an oven set at 80 °C to produce a brown powder of AgNPs and a deep red powder of SeNPs.

Characterizations of NPs

UV–Vis Spectrum Analysis: As shown in Figure 1, the synthesis of AgNPs in the reaction mixture was confirmed by UV-visible spectrophotometry, which showed a peak at 400 nm, as described by Dakhil (2017). Stimulating the surface plasmon vibrations of the metal nanoparticles turned them brown, as is typical for AgNPs. UV-Vis spectroscopy was used to prove the biosynthesis of SeNPs by taking readings at wavelengths ranging from 360 to 600 nm. Figure 1 did not show any peak that could be the SeNPs surface Plasmon resonance (SPR). As stated in Lin and Wang (2005), SeNPs that are smaller than 100 nm do not show an identifiable peak (λ_{max}) between 200 and 800 nm.

Transmission Electron Microscopy (TEM): Biosynthesized NPs' size and shape, along with other morphological features, were investigated using transmission electron microscopy (TEM). Figure 2A shows that the NPs that were produced were spherical, well-distributed, and free of aggregates.

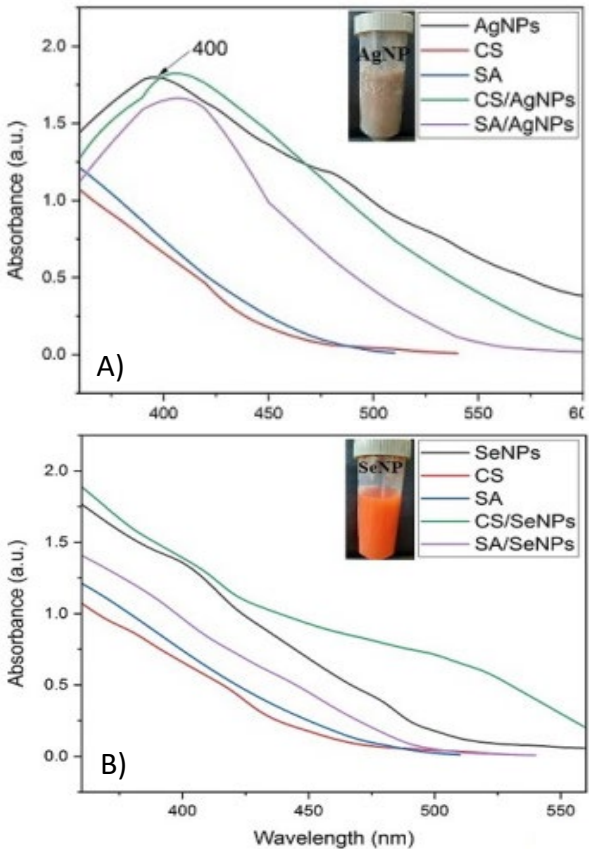

Figure 1. UV-Visible spectrophotometry of (A) AgNPs and (B) SeNPs with their nanocomposite films. AgNPs: silver nanoparticles, SeNPs: selenium nanoparticles, CS: chitosan, SA: sodium alginate.

The average size of AgNPs was 6.41–11 nm, and their polydispersity index (PDI) was 0.643. On the other hand, the majority of SeNPs were 32.3–50.7 nm in size, and their PDI was 0.29. This study's findings are like those of previous research. According to Mohammed et al. (2024), TEM investigation of the mycosynthesized *Embellisia*-AgNPs and *Gymnoascus*-AgNPs, showed that they are equally distributed spherical nanoparticles with a diameter ranging from 2 to 20 nm with PDI of 0.28 and 0.40, respectively. Fath-Alla et al. (2024) used *Saccharomyces cerevisiae* to biosynthesize SeNPs. The particle size ranged from 34 to 125 nm, and their PDI value was 0.503. The particle shape was spherical.

Dynamic Light Scattering (DLS): The average particle size for NPs formed by the *Aspergillus ochraceus* NSRN22 strain was shown in Figure 2B, according to DLS analysis. Biomoieties attached as stabilizers, substances absorbed on the NPs' surfaces, and the metallic core of the NPs all impact the size determined by DLS (Salem et al., 2021). Results from DLS showed that the average size of AgNPs was 68 nm and their zeta potential was -22.2 mV, suggesting that the AgNPs are very stable owing to the electrostatic repulsion between them, as shown in Figures 2B and 2C. Previous studies have demonstrated that biosynthesized AgNPs typically contain negatively charged groups, which could account for their negative zeta potential value (Elamawi et al., 2018). In the present work, the SeNPs that were examined had an average size of 68 nm. One way to measure the surface charges of nanoparticles in a colloidal solution is by examining their zeta potential. The observed zeta potential of SeNPs was -30.7 mV. These findings are consistent with what Qiao et al. (2022) found. They biosynthesized AgNPs with a zeta potential of -25.58 mV and an average particle size of 50.28 nm, as determined by DLS analysis. Meanwhile, a zeta potential of -22.4 mV and a size of 173.9 nm were the results of DLS analysis of SeNPs made by Fath-Alla et al. (2024).

FT-IR Spectroscopy: The produced NPs were freeze-dried before FT-IR spectroscopy could be performed. The FT-IR spectra of the NPs biosynthesized by the *Aspergillus ochraceus* NSRN22 biomass filtrate are displayed in Figure 3A. Fourier transform infrared spectroscopy was utilized to find ion-metabolite interactions in biomass filtrate. These metabolites may act as a reducing intermediary and capping agent, leading to the formation of well-dispersed NPs in their colloidal solution. The amide bonds between amino acid residues in proteins are known to produce

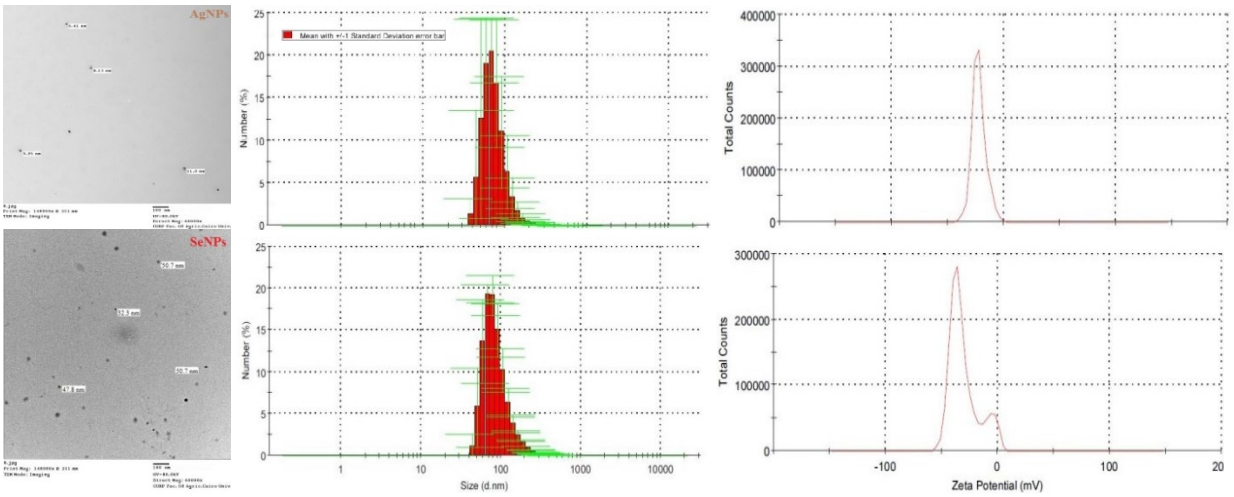

Figure 2. (A) TEM, (B) Particle size distribution, and (C) Zeta potential for the biosynthesized AgNPs and SeNPs. AgNPs: silver nanoparticles, SeNPs: selenium nanoparticles.

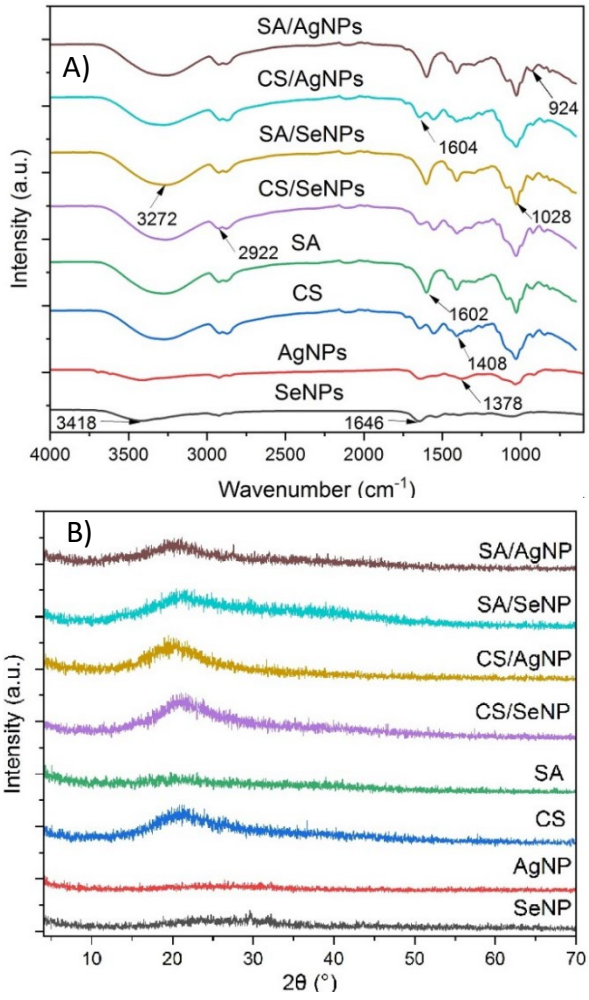

Figure 3. (A) FTIR and (B) XRD of AgNPs, SeNPs, CS, SA, CS/SeNPS, CS/AgNPs, SA/SeNPs and SA/AgNPs film samples. AgNPs: silver nanoparticles, SeNPs: selenium nanoparticles, CS: chitosan, SA: sodium alginate.

visible infrared fingerprints (Jain et al., 2011). Proteins or other hydroxyl functional groups may have caused the peaks at 3418 cm^{-1} due to their strong stretching vibrations (Priyadarshini et al., 2013). The bands at 2922 cm^{-1} may indicate the C-H stretching of the methylene groups in proteins, as suggested by (Ghaseminezhad et al., 2012). Bands at 1028 cm^{-1} and 1646 cm^{-1}, respectively, indicate protein amide linkages (amide I and amide II), which are responsible for the -N-H and carbonyl C-O stretching vibrations, respectively, as shown in (Suresh et al., 2011). The peaks at 1378 cm^{-1}, on the other hand, could represent the COO-symmetrical stretch from the carboxyl groups of amino acid residues, as suggested by Gajbhiye et al. (2009). According to Gopinath and Velusamy (2013), the carboxyl groups of Asp and Glu residues, as well as the hydroxyl groups of Tyr residues, are the most active functional groups for Ag reduction and the anisotropic development of AgNPs. On the other hand, in infrared spectra taken by the biosynthesized SeNPs, O-H stretching groups of phenols and alcohols are associated with the peak at 3418 cm^{-1}, which may be due to the N-H asymmetric stretch mode of amines (El-Sayyad et al., 2020). However, the 1536 cm^{-1} band is correlated with the binding vibrations of the protein's amide I band with N-H stretching. The peak at 1079 cm^{-1} is caused by a stretching vibration of the C-O bond (Zhang et al., 2019). All the above proves that the metabolites made by the *Aspergillus ochraceus* NSRN22 biomass filtrate are important to produce SeNPs.

XRD Analysis: Silver nanoparticles, greenly synthesized by *Aspergillus ochraceus* NSRN22, are

shown in Figure 3B as an XRD pattern. The Bragg's diffraction peaks for the green synthesized AgNPs were determined to be 38.02°, 45.8° and 77.1°, respectively. According to Qiao et al. (2022), these two prominent XRD peaks represent planes (111), (200) and (311), respectively. This showcases the face-centered cubic (FCC) structure and crystallinity of AgNPs made from *Aspergillus ochraceus* NSRN22. Figure 3B shows the XRD pattern of the SeNPs, which reveals their hexagonal structure. The diffraction peaks 2θ at 23.6°, 29.9°, 41.4°, 43.8°, 45.4°, 51.8°, 55.9°, 61.8°, 65.3° and 68.3° were symbols of the typical Bragg's reflections at angles (100), (101), (110), (102), (111), (201), (003), (202), (210) and (211), respectively (Srivastava and Mukhopadhyay, 2015). The results of the XRD pattern confirm that the substance listed in the ICDD file number 00-001-0848 is elemental selenium.

Antifungal activity of synthesized NPs

The isolated *Penicillium citrinum* was utilized to test the antifungal potency of AgNPs and SeNPs. The absence of *Penicillium citrinum* spore germination was caused by the produced NPs. The MIC values for itraconazole, selenium nanoparticles, and silver nanoparticles were 200, 100, and 50µg/mL, respectively. The antimicrobial efficacy of AgNPs has been demonstrated in earlier studies. The mechanism by which AgNPs exert their antimicrobial properties was better understood after studies examined the possible loss of DNA and proteins. Scientists discovered that the presence of AgNPs caused proteins and DNA to leak out of the spore solution. The majority of AgNPs, as stated by Durán et al. (2016), attach to specific sites on the cell membrane and then readily penetrate it, creating pores that enable substances to exit the cell. Consequently, DNA and proteins were released from the tested fungal cells.

In this research, SeNPs demonstrated a potent antifungal activity at a concentration of 100µg/mL by inhibiting the germination of fungal spores. Research has demonstrated that SeNPs can inhibit the growth of specific types of fungi when used at lower concentrations. For instance, El-Saadony et al. (2021) found that the effects of SeNPs derived from chemical and environmentally friendly methods on *Fusarium graminearum*, *F. cereales*, *F. poae*, *F. avenaceum*, *and F. culmorum* were examined. In this research, SeNP concentrations varied between 50 and 150µg/mL. In terms of controlling the examined fungi, the results demonstrated that fungal growth was considerably inhibited in the MIC range (25-45 µg/mL) by the ChemSeNPs. On the other hand, BioSeNPs effectively inhibited the tested fungi within the 20-40 µg/mL MIC range. A probable theory is that the stability and surface area/volume ratio of the bulk form of the same material prevent it from exhibiting the same antibacterial capabilities as smaller-size nanoparticles. Nanoparticles (NPs) can bind to the cell membranes of microorganisms due to their small size and high surface area to volume ratio. This provides opportunities for diffusion and interactions within cells, which stimulate processes mediated by reactive oxygen species (ROS) that either damage DNA or restrict cell proliferation. Or maybe the ions that NPs release into the environment are responsible for their antimicrobial effects. The rate of ion dissolution is supposedly determined by the concentration of the solution and the size of the NPs (Lazcano-Ramírez et al., 2023).

Preparation and Characterization of nanocomposite films

The color of the film used for covering food affects how the product looks and how a customer perceives it. The color of films made of either chitosan or SA varied from colorless transparency to yellow in the presence of AgNPs and red in the presence of SeNPs.

UV–Vis Spectrum Analysis: The optical properties of the chitosan composite films were investigated using transmission ultraviolet-visible spectrophotometry. Figure 1 shows that CS film had the lightest transmission in the visible and ultraviolet light spectra. Specifically, at a wavelength ranging between 360- and 600 nm, there are no light-blocking particles or functional groups, which lead to this result (Ediyilyam et al., 2021). Adding silver nanoparticles to CS (CS/AgNPs), on the other hand, made them absorb light more effectively. It is the result of the nanoparticle coating's absorbing groups working in harmony with the light-blocking or scattering effect. The CS/SeNPs film achieved the lowest UV-Vis light transmission. This occurs because, once dispersed into the CS substrate, SeNPs can either scatter or block light as it is transmitted through the film. It can thus be suggested that packaged foods could be protected from light-induced quality losses by using the CS/SeNPs coating since it successfully blocked UV-Vis light. By examining their UV-Vis absorption spectra, one could determine whether the AgNPs were stable within the film. Figure 1 shows that the SA/AgNPs film did display an absorption peak, which corresponds to the absorption peak of AgNPs; in

contrast, the SA film showed almost no noticeable absorption peak. Research demonstrated that AgNPs were able to keep their shape while embedded in the film.

FT-IR: Figure 3A shows the chitosan films with the asymmetric stretch mode of the amines and the stretching vibration peaks of the -OH limits in the absorption bands at 3272 and 3265 cm^{-1}. Amide-I and amide-II linkage bending results in an absorption band at 1640 cm^{-1}, which is caused by the presence of residual N -acetyl groups. In $-CH_3$, the peak at 1408 cm^{-1} corresponds to the angular vibration of $-(CH_2)n-$. The band at 1028 cm^{-1} shows the stretching of the C-O skeleton. The bands at 2922 and 2929 cm^{-1} in SA films are linked to the stretching vibrations of the methylene groups. As can be seen from the absorption peak at 1408 cm^{-1}, the stretching vibration of the carboxylate anion -COO- demonstrates two characteristics: the asymmetric and the symmetric stretching vibrations of the carboxylate group. The vibration at 1028 cm^{-1} reflects the C-O stretching in the carboxylic groups of the SA backbone. When polysaccharides are present, the stretching of C-O-C bonds is indicated by the band at 924 cm^{-1}. Finally, the C-N stretching band is at 1326 cm^{-1}, while the amide I and II bands are at 1640 and 1558 cm^{-1}, respectively. The fingerprint region highlights the saccharides structure through absorption peaks at 850 and 1252 cm^{-1} (Schulz and Baranska, 2007).

Water contact angle: A film containing AgNPs or SeNPs was created by combining Sodium Alginate or Chitosan nanocomposites. The water contact angle is represented in Figure 4A. The films made of SA/nanocomposites exhibited a highly hydrophilic surface and significantly low contact angles. Films made of SA/nanocomposite materials had extremely low contact angles, which is consistent with previous research and suggests that alginate films show super hydrophilicity (Xu et al., 2016). The hydrophobic properties and high-water contact angle of chitosan film surfaces have been previously documented (Luo et al., 2014). The water contact angle of 27.02° observed in the present investigation is moderate for CS/SeNPs films. In contrast to CS/SeNPs films, CS/AgNPs films exhibited an extremely low water contact angle. The wettability of chitosan films is indicated by CS/nanocomposite films with extremely low contact angles. It is worth to mention that in addition to preventing denture stomatitis, it greatly aids in reducing bacterial adhesion (Tang et al., 2023).

SEM with EDX: Scanning electron micrographs (SEM) captured of nanocomposite films at different magnifications are shown in Figure 4B. Films were non-porous, non-homogeneous, and non-smooth with straps and shrinkages and included spherical, amorphous, and consistent particle sizes of nanoparticles. An EDX analysis was performed to identify the chemical composition of the final hybrid nanocomposite. Carbon and oxygen were the main ingredients in the sample for chitosan nanocomposite films. On the other hand, films made of sodium alginate nanocomposite showed three separate signals for the alginate molecule's C, O, and Na components. The appearance of the Se and Ag peaks in the EDX-spectra, indicating the presence of NPs in the films, proved that chitosan and alginate are applicable substrates for dispersing NPs.

XRD: Using XRD analysis, the structures of the films were further explained. Figure 3B shows the XRD patterns of films that contain various nanoparticles (NPs): CS, SA, SA/SeNPs, SA/AgNPs, CS/AgNPs and CS/SeNPs. The peaks at 2θ of 17.9° (101), and 22.3° (102) shown by the CS films correspond to the semicrystalline phase of CS, as illustrated in Figure 3B. Bond peaks between 13 and 20° reflected the film's amorphous structure, which is typical of chitosan (Qin et al., 2019). The peak of chitosan was changed when AgNPs and SeNPs were added to the film. Even though they were flatter and less noticeable, the diffraction peaks remained. One possible explanation is that the presence of nanoparticles interfered with the ability of chitosan to form intramolecular interactions, leading to a more amorphous complex due to the competitive influence of hydrogen bonds between the two molecules (Dong et al., 2022). The produced alginate biopolymer's XRD pattern reveals its amorphous structure. The SA/SeNPs product's XRD pattern revealed diffraction peaks at 28.09° (100) and 29.25° (101). As previously mentioned, the pure AgNPs exhibited diffraction peaks at 2θ= 38.02° and 46.1°. However, when AgNPs were added to the SA film, these unique peaks disappeared. These results are in agreement with those of the previous study of (Li et al., 2022).

Mechanical properties: The mechanical strength of the packaging system plays an important role in protecting food throughout stressful environments such as storage, handling, and processing. The mechanical properties of the film used to package active foods should be carefully considered to ensure that the film does not crack while in transit or storage.

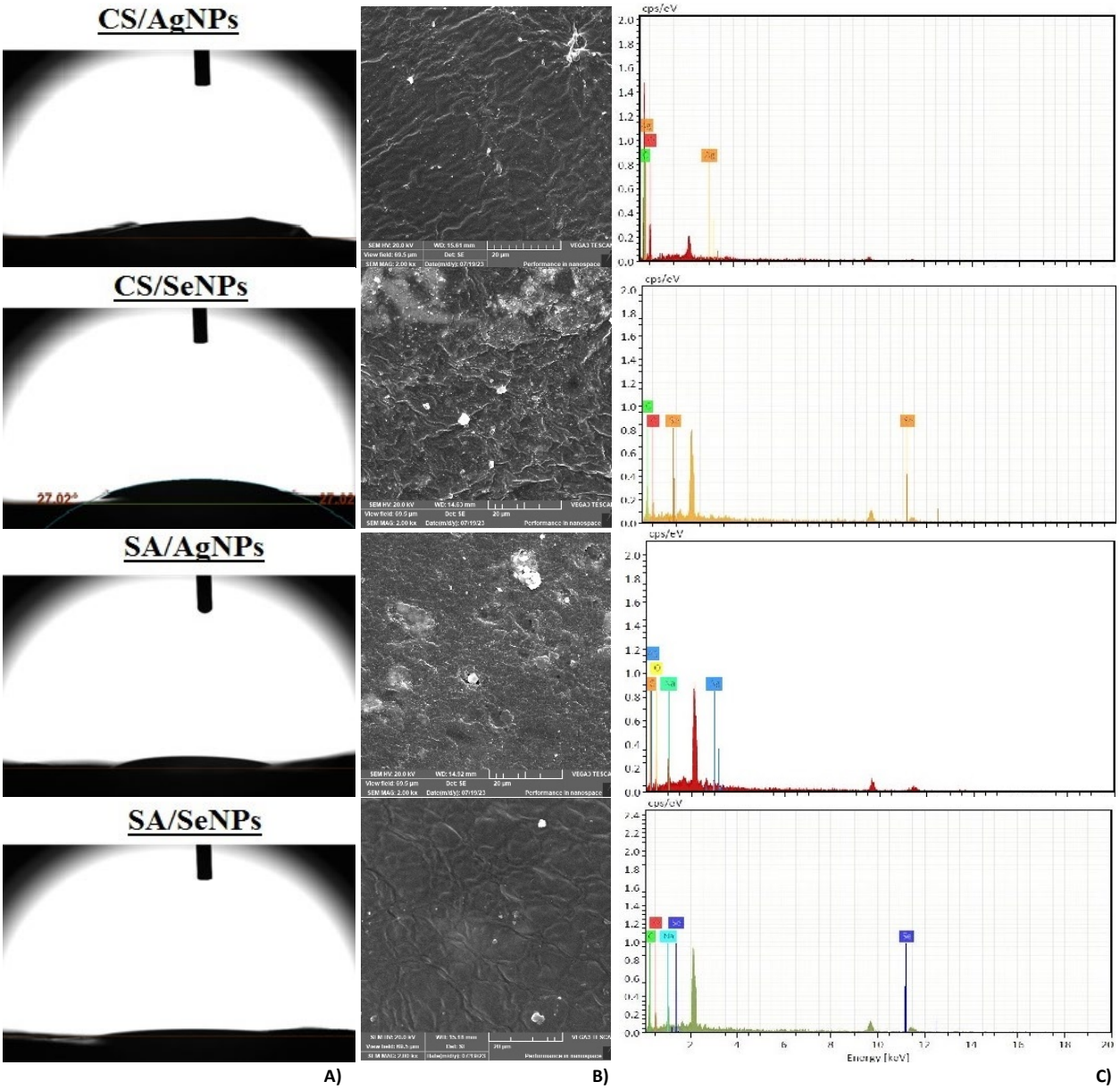

Figure 4. (A) Water contact angle, (B) SEM image and (C) EDX of CS or SA composite films with AgNPs or SeNPs. AgNPs: silver nanoparticles, SeNPs: selenium nanoparticles, CS: chitosan, SA: sodium alginate.

Table 1. Thickness, Elongation at break (EAB), Tensile strength (TS) Moisture content (MC), Water solubility (WS) and Water Vapor permeability (WVP), of CS, SA films and composite films with either SeNPs or AgNPs.

Sample	Thickness (mm)	Elongation at break (EAB) (%)	Tensile strength (TS) (MPa)	Moisture content (MC) (%)	Water solubility (WS) (%)	Water Vapor permeability (WVP) ($g/m^2.day$)
Chitosan	0.26 ± 0.03^{d}	2.52 ± 0.67^{a}	0.58 ± 0.17^{a}	13.24 ± 1.08^{a}	40.22 ± 1.34^{b}	2021.57 ± 2.60^{e}
SA	0.22 ± 0.026^{c}	70.55 ± 3.71^{d}	2.42 ± 0.36^{b}	23.66 ± 1.52^{c}	92.33 ± 2.51^{f}	2132.59 ± 3.38^{f}
CS/AgNPs	0.12 ± 0.017^{a}	9.54 ± 0.35^{b}	4.15 ± 0.27^{d}	11.79 ± 2.57^{a}	47.81 ± 2.28^{c}	1559.94 ± 4.35^{b}
CS/SeNPs	0.24 ± 0.026^{cd}	9.21 ± 0.64^{b}	4.16 ± 0.23^{d}	12.33 ± 2.51^{a}	20.06 ± 1.19^{a}	1518.93 ± 3.70^{a}
SA/AgNPs	0.17 ± 0.005^{b}	64.22 ± 1.19^{c}	3.07 ± 0.29^{c}	21.50 ± 0.46^{c}	89.29 ± 4.04^{e}	1945.24 ± 5.11^{d}
SA/SeNPs	0.14 ± 0.026^{ab}	62.74 ± 2.23^{c}	2.48 ± 0.41^{b}	16.84 ± 1.41^{b}	83.66 ± 0.61^{d}	1775.96 ± 5.05^{c}
LSD	0.04	3.23	0.52	3.04	4.08	7.12

Data are means ± SD. SD: standard deviation. Values with similar superscript letters are insignificantly different while the different superscript letters are significantly different. LSD is the least significant difference at $p \leq 0.05$.

The mechanical properties of an active film are defined by the film matrix's intramolecular structure and the filler-film interaction (Perera et al. 2022). The study's findings, presented in Table 1, show how the addition of AgNPs and SeNPs affected the tensile strength (TS) and elongation at break (EAB) mechanical properties of films made of chitosan and sodium alginate. Out of all the films tested, the chitosan film without nanoparticles had the lowest TS (0.58 MPa) and EAB (2.52%). The TS of the CS films was significantly improved ($p \leq 0.05$) after SeNPs or AgNPs were added to them. Films containing AgNPs have a TS of 4.15 MPa and an EAB of 9.54%. After adding SeNPs to the film, the TS increased to 4.16 MPa and the EAB to 9.21%. When it came to SA films, the ones without NPs showed the highest EAB (70.55%) and TS (2.42 MPa). The films that contain AgNPs have a TS of 3.07 MPa and an EAB of 64.22%, while the films that contain SeNPs have a TS of 2.48 MPa and an EAB of 62.74%. This study has demonstrated that there is no significant difference between CS/SeNPs films and CS/AgNPs films but the TS and EAB were improved when compared to alginate films. The addition of SeNPs or AgNPs in alginate films considerably decreased the EAB of films ($p \leq 0.05$), as was observed. Intermolecular forces and network structure are known to impact film mechanical properties. The addition and uniform distribution of SeNPs or AgNPs may have enhanced their interaction with chains of macromolecules, which could explain the result. For the same concentration of NPs, films containing nanoparticles exhibited higher TS. This is because the mechanical strength of the film is enhanced by the nanoparticles, due to their small size. this produces a more comprehensive network structure and ensures that external forces are distributed more uniformly on the film matrix (Dong et al., 2022). Nanocomposite films' EAB tends to decrease when metal or metallic nanoparticles are combined with biopolymer films, especially if the nanofiller and polymer matrix are not suitable to one another. Nanocomposite films' EAB improves as the strength of the interaction between the nanofiller and the polymer matrix is greater than that between the polymeric chains (Shankar et al., 2016).

Thermal analysis: Thermogravimetric analysis (TGA) is a common way to find out how thermally stable a film is. Figure 5 shows the TGA curves. The curves demonstrate three separate stages. All samples were found to have a weight reduction between 25 and 130 °C after the first step of removing bound water and physical adsorption (Li et al., 2024). As the polymer chain's functional groups broke down between 130 and 400 °C, a significant weight loss occurred during the second stage. The degree of reduction in each sample was different. Decomposition, which took place at temperatures ranging from 130 to 400 °C, led to a progressive loss of weight for the following samples: CS (73%), SA (78%), CS/AgNPs (70%), CS/SeNPs (69%), SA/AgNPs (76%), and SA/SeNPs (75%). The amine, carboxyl, and hydroxyl polar groups found in both chitosan and sodium alginate give them the ability to bind water molecules (Kulig et al., 2016). The mass decrease at this stage could be due to the release of water molecules and volatile compounds linked to them if the biopolymer's functional groups were not removed in the first phase. Biopolymers also undergo mass loss at these temperatures because of carboxyl group breakdown. Mass loss caused by biopolymer chain depolymerization is also possible within this temperature range. The temperature range of 200 to 300 °C was the principal region of thermal degradation. The main reasons for this were the thermal breakdown of the polymer matrix and the volatilization of glycerol, a substance with a boiling point of 289 °C (Shankar et al., 2016). Mass loss occurs between 450 and 600 °C due to SA biopolymer degradation to Na_2CO_3 and complete organic component elimination (Soares et al., 2004). The TGA results showed that the selenium and silver nanocomposite films significantly enhanced thermal stability compared to the control films made of chitosan and alginate composite. In addition, compared to the other samples, CS/SeNPs exhibited

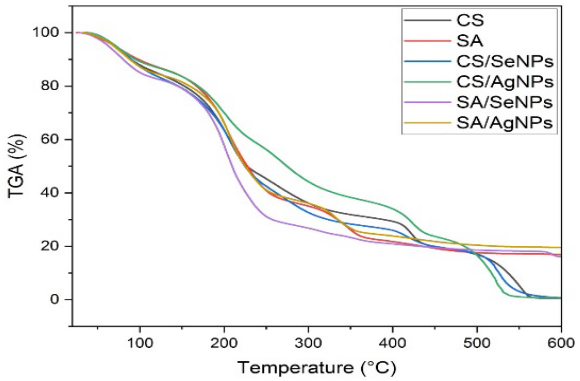

Figure 5. Thermogravimetric curves of CS, SA, CS/SeNPs, CS/AgNPs, SA/SeNPs and SA/AgNPs films. AgNPs: silver nanoparticles, SeNPs: selenium nanoparticles, CS: chitosan, SA: sodium alginate.

the highest thermal stability, as evidenced by their lowest mass loss rate. The additives used to construct the structure increase the pyrolysis residue and postpone the films' slow decomposition. Because these films are more stable at high temperatures, they are very useful in the food industry.

Moisture content (MC) and water solubility (WS): One approach to evaluate the water resistance of films used for food packaging is to measure their water solubility and moisture content. Table 1 shows that the CS film had a high solubility of 40.22% and a moisture content of 13.24%, indicating that it was highly hydrophilic. It is possible that the addition of SeNPs and AgNPs caused a significant increase ($p \leq 0.05$) in the films' moisture content and water solubility. This is likely due to the presence of additional hydrophilic groups in the coating molecules of these nanoparticles. The water solubility of the chitosan film decreased from 40.22% to 20.06% following the addition of SeNPs, which are insoluble in water. There appears to be a strong bond between the two functional groups in CS/AgNPs because they are more water-soluble than chitosan. Several studies found that the solubility of chitosan films changed when solid nanoparticles were added, so it was assumed that the crosslinking action of the particles and the intermolecular bonding of chitosan chains were responsible for the stability or reduction of this feature. As a result, lessening the impact of crosslinking can increase solubility (Ediyilyam et al., 2021). At 92.33%, SA's water solubility was the highest among the evaluated films. Solubility was strong in both the SA/AgNPs film (89.29%) and the SA/SeNPs film (83.66%), even though the SA film was stronger. The formation of strong hydrogen bonds between the film matrix and the NPs is primarily responsible for the decrease in the film's water solubility and moisture content. To make the biopolymer matrix more cohesive and less water sensitive, the hydroxyl groups of the extract-capped NPs may form strong hydrogen bonds with the hydroxyl and carboxyl groups on alginate (Gudimalla et al., 2022).

Water vapor permeability: One of the many factors influencing food qualities is water vapor pressure (WVP). One way films with low water vapor transmission (WVP) can prolong the freshness and quality of food by reducing the water exchange between the food and its environment. Keeping the WVP as low as possible will prevent food from becoming dehydrated, according to (Chen et al., 2024). The WVPs of different films are shown in Table 1. Adding SeNPs or AgNPs significantly decreased the films' WVP ($p \leq 0.05$), even though the SA film had the highest WVP. The film content of CS decreased from 2021.57 g/m^2.day to 1559.94 g/m^2.day for CS/AgNPs and 1518.93 g/m^2.day for CS/SeNPs. SA Films containing AgNPs reduced WVP from 2132.59 to 1945.24 g/m^2.day, while films containing SeNPs reduced it to 1775.96 g/m^2.day. Adding SeNPs or AgNPs to the films may enhance their water barrier properties. Nanoparticles can form a dense network structure by filling the pores of the film matrix. Since this causes the water molecules to take a longer route through the film matrix, their diffusion is reduced (Dong et al., 2022). Consistent with what was found in the film's scanning electron microscopy (SEM) analysis, this points to the fact that nanoparticles make the film denser and that their small size makes them easier to evenly distribute into macro molecule chains, thus improving the film's barrier properties. Interactions between surface molecules and CS functional groups and hydroxyl groups occur in biosynthesized SeNPs and AgNPs. Among the most likely major reasons for these points are the following: the nanoparticles obstructed the micro-paths of water vapor in the film networks, and the incorporation of water-insoluble nanoparticles into CS film produced an additional, very thin protective layer, both of which could improve the barrier properties of nanocomposite films (Soltani et al., 2023). Dense networks can be formed by SeNPs or AgNPs interacting with the hydrophilic groups of CS. This makes the material highly resistant to the absorption of water vapor and improves its barrier properties.

Antioxidant activity

In this study, the films' ability to scavenge 1,1-diphenyl-2-picrylhydrazl (DPPH) radicals was examined. The DPPH radical scavenging test is based on the reduced DPPH level. The purple stable free radical DPPH, which is centered around nitrogen, shows a peak at 517 nm. The absorbance and color intensity are reduced because antioxidants neutralize the free radicals in DPPH (Baliyan et al., 2022). Figure 6A shows that all of the tested films had antioxidant capabilities. The absence of nanoparticles in the CS film did not affect its DPPH radical scavenging activity. This is likely because free amino and hydroxyl groups in CS react with free radicals to form very stable ammonium groups and macromolecular free radicals (Li et al., 2019). Composite films enhanced with SeNPs and AgNPs DPPH radical scavenging capabilities were found to be significantly higher than those of the chitosan film (22.1%) and SA (18.25%).

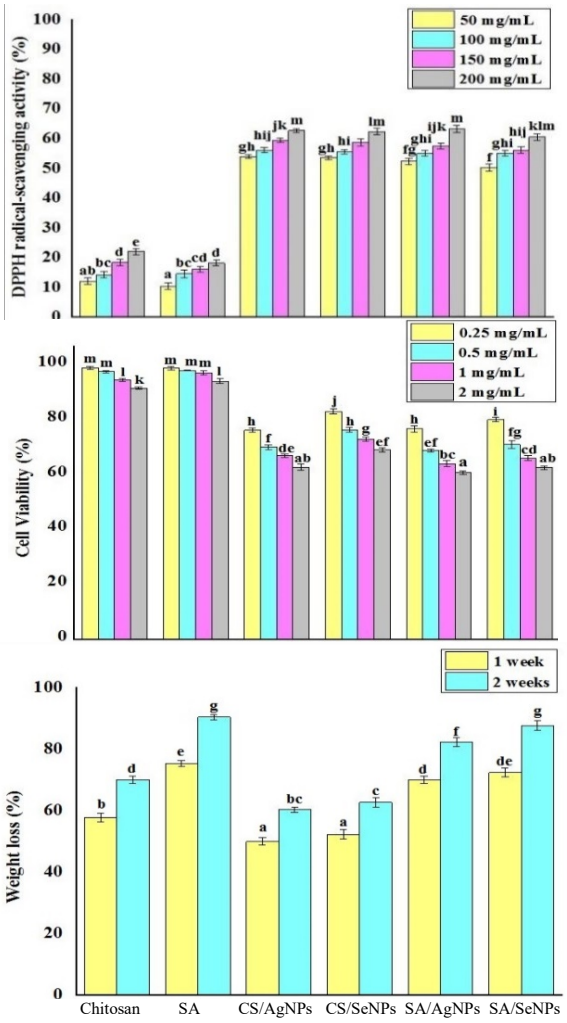

Figure 6. (A) DPPH radical-scavenging activity (%), (B) Cytotoxicity assay of cell survival of the BHK (normal cells) as a function of chitosan and alginate/nanocomposite films and (C) Biodegradability of CS, SA, CS/SeNPS, CS/AgNPs, SA/SeNPs and SA/AgNPs films. The results are the means of three replicates. Bars show means. Error bars show mean ± SE. Values with similar superscript letters are insignificantly different while the different superscript letters are significantly different. LSD for DPPH radical-scavenging activity= 2.868 at $p \leq 0.05$, LSD for Cytotoxicity= 2.35 at $p \leq 0.05$ and LSD for Biodegradability= 3.634. AgNPs: silver nanoparticles, SeNPs: selenium nanoparticles, CS: chitosan, SA: sodium alginate.

The highest DPPH radical scavenging activity, reaching 63.3%, was observed in films that contained both SA and AgNPs. Films containing AgNPs or SeNPs demonstrated enhanced DPPH radical scavenging capabilities when added to CS films (62.68% and 62.42%, respectively). Composite films' DPPH radical scavenging activity was enhanced by adding NPs with this property. NPs may enhance the film's antioxidant activity by accepting or donating electrons. Both SA/AgNPs and CS/AgNPs possess high antioxidant properties due to the presence of silver nanoparticles, which are well-known for their antioxidant capabilities. It is important to mention that the NPs used in this study were made using a green method that depended on fungal extract. The particles are coated with compounds to enhance their antioxidant activity in this approach. When NPs were added to the films, the DPPH radical scavenging activity significantly increased ($p \leq 0.05$). As suggested by Nunes et al. (2018), the bioactive capping agents on the AgNP surfaces were responsible for the CS/AgNPs film's enhanced antioxidant activity. Preventing degenerative diseases caused by free-radically induced oxidation of packaged foods is a promising application for CS/AgNPs and SA/AgNPs film. The highest level of DPPH radical scavenging activity was shown in these films.

Cytotoxicity

Materials used for producing packaging should be low in cell cytotoxicity (Wahab et al., 2024). In MTT experiments, the cytotoxicity of composite films made of chitosan and sodium alginate was evaluated by examining cell viability. After the samples were added to the medium, every film showed promising cell viability. Figure 6B demonstrates, however, that as the film content increases, various films exhibit markedly diverse cell viability. It is notable that at a concentration of 2 mg/mL, the cell vitality of CS/AgNPs films was 63%, whereas the cell viability of CS/SeNPs films was 69.3% and that of pure CS films was 91.8%. There is a marked difference in the toxicity to the BHK cells between CS/AgNPs films and CS/SeNPs films. The results demonstrate that the cytotoxic effect was reduced when SeNPs were immobilized on chitosan. The cytotoxicity of films containing SeNPs was reduced in SA/SeNPs, which prevented bare nanoparticles from interacting with cellular components and had 62.8% cell vitality. Human exposure to chitosan has been documented in dietary supplement formulations for obesity and hypercholesterolemia (Ilium, 1998). Chitosan and alginate are safe to use in food because they have the GRAS (generally recognized as safe) designation from the US Food and Drug Administration (Luo and Wang, 2013; Heydari et al., 2015). According to the European Food Safety Authority (EFSA), alginate and related salts can be used in limited doses (Gheorghita et al., 2020). Thus, the composite films showed strong cytocompatibility and high cell viability, making them safe for use in the food industry.

Biodegradability in soil

Researchers perform biodegradability studies to learn how films behave in the environment and whether they contribute to pollution. Soil burial is one of these methodologies. There is a rapid rate of breakdown at the initial stage of degradation due to high microbial activity; thereafter, the rate of degradation moderates during the curing period. The degradation of the nanocomposite films after a week is shown in Figure 6C. The first section demonstrates the effects of water absorption into the polymeric network on the films' physical characteristics, specifically how the SA and CS chains have been damaged. The CS film may have lost up to 70% of its weight after two weeks of soil exposure, while the SA film may have lost up to 90.33% (Figure 6C). Composite films biodegraded differently after SeNPs and AgNPs were added. Supplementing SA or CS with SeNPs or AgNPs slowed their degradation rate. Selenium and silver nanoparticles' antibacterial activity is the main reason why CS/AgNPs (60.33%), CS/SeNPs (62.67%), SA/AgNPs (82.33%) and SA/SeNPs (87.67%) do not degrade very quickly. Accordingly, degrading microbes are unable to grow (Kale et al., 2007).

Antifungal activity of nanocomposite films

It is thought that nanoparticles (NPs) are effective against fungi because they either penetrate their cells and disrupt their internal processes or damage their cell walls. Polysaccharide components such as chitin, glucan, and chitin-glucan complexes form the cell walls of fungi and act as a defense mechanism against outside influences. NPs have the potential to cause cellular homeostasis and apoptosis by damaging cell membranes and interfering with diffusibility. NPs can increase ROS production, which in turn can lead to oxidative stress (Nikzamir et al., 2021). Safaei et al. (2019) brought attention to the fact that NPs can bind to DNA, and disrupt intercellular organelles like lysosomes, endoplasmic reticulum, ribosomes, and mitochondria, leading to cell death. Chitosan is a common food additive with antimicrobial characteristics that can be utilized to treat food after harvesting. Positively charged CS molecules exert their antimicrobial action by electrostatically interacting with negatively charged outer fungal cell membranes (Xing et al., 2021). In the long term, this additive can protect food by inducing resistance against microorganisms. Chitosan edible coatings control moisture transfer, delay respiration and oxidation, and lengthen the duration of storage life of vegetables (Riseh et al., 2023). On the other hand, alginate biopolymer's antifungal efficacy remains unproven. Nanocomposites with antifungal properties, such as Ag and Se nanoparticles, can be created by using alginate biopolymer as a matrix (Hurtado et al., 2022). In the present work, in terms of controlling *Penicillium citrinum*, it was expected that the CS/AgNPs solution would perform better than CS alone (MIC of 1160 µg/ 5 mL). As shown in Figure 7, the minimum inhibitor concentration causing antifungal activity for CS/AgNPs was 1020 µg/ 5 mL. It was the strongest of the solutions tested against the fungus. In comparison, solutions containing SA, CS/SeNPs, SA/AgNPs, and SA/SeNPs were slightly weaker, with MIC effects of around 1160, 1040, 1080, and 1025 µg/ 5 mL, respectively.

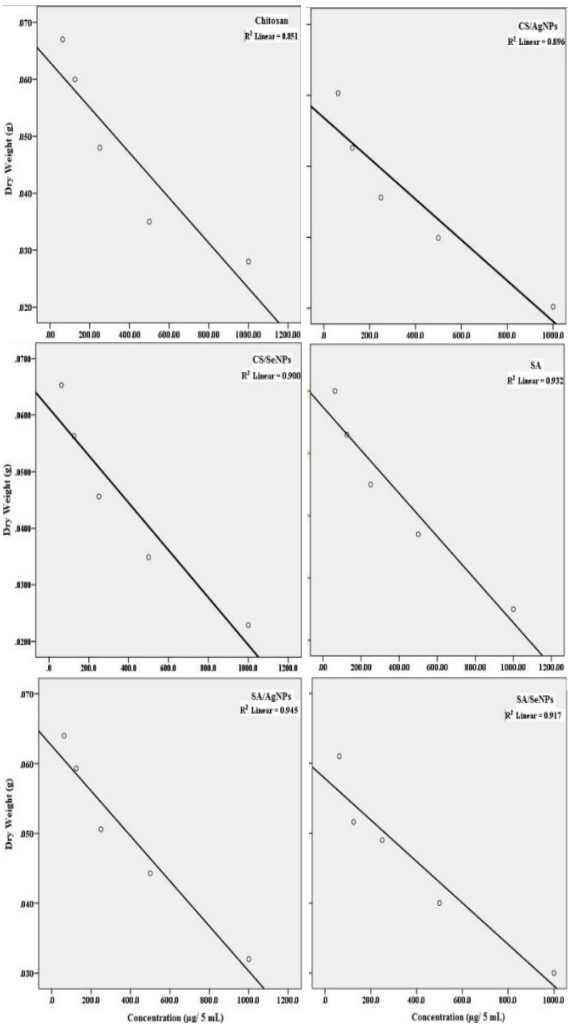

Figure 7. Linear regression model fit of antifungal activity of CS, SA, CS/SeNPs, CS/AgNPs, SA/SeNPs and SA/AgNPs to determine the MIC value. AgNPs: silver nanoparticles, SeNPs: selenium nanoparticles, CS: chitosan, SA: sodium alginate.

Packaging efficiency of nanocomposites films

To keep food fresh for a longer time and reduce spoilage, films are essential in food packaging. Many things can affect food quality: the coating, the storage conditions, rotting, fruit water content, weight loss, evaporation, and the degradation of organic acids and carbohydrates by oxidation (Shiekh et al., 2021). Because of their high inhibitory effect against microorganisms CS and SA films of AgNPs or SeNPs are good materials for food packaging; they successfully prevent water evaporation and respiration in fruits. The significance of films in avoiding food spoilage and maintaining food quality is emphasized in this study. Testing at regular intervals the effect of the active films on lemons was evaluated over a 20-day storage period at temperatures between 5 and 8 °C. In this case, the control was the market film. In Figure 8, it is observed that the lemon's visual impact declined with time in storage. Shehata et al. (2021) found that wilting, shrinking, color change, and deterioration during storage can cause a decrease in appearance. Films containing CS/SeNPs, CS/AgNPs, SA/SeNPs, and SA/AgNPs improved the appearance and shelf life of lemons for up to 12 days (Figure 8).

In addition to not showing any indications of rotting or liquid leaking from them, these lemons had a smooth surface. After six days, the market film developed white spots, which indicated a fungal infection. After 20 days, the combination of CS and SeNPs resulted in the lowest weight loss (2.13%) in lemons, compared to the weight loss of 2.69% for CS/AgNPs, 2.89% for SA/AgNPs, and 2.70% for SA/SeNPs. Owing to their ability to facilitate the antimicrobial agents' direct interaction with the food, composite films are excellent nanoparticle carriers. When food comes into touch with silver nanoparticles (AgNPs), the nanocomposite films slowly release the AgNPs, preventing microbes from penetrating the packaging (Ediyilyam et al., 2021). The edible CS/SeNPs coating successfully inhibited mold growth while maintaining lemons' initial appearance. The covered lemons kept their freshness even after a 12-day storage period. Brown spots appeared on the SA-coated sample 10 days after coating, despite SA's antimicrobial characteristics. It is possible that SA's free hydrophilic functional groups made it easier for airborne water molecules to bind, which in turn made fruit surfaces more moist and created an ideal environment for fungal growth (Nair et al., 2020).

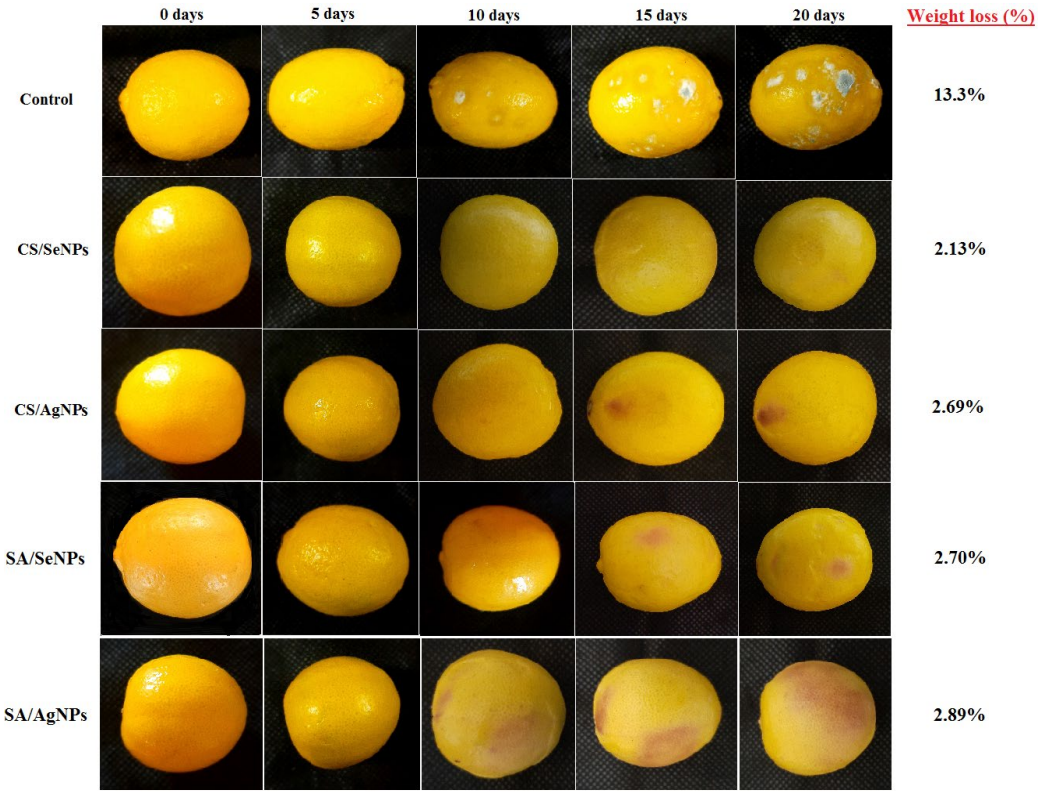

Figure 8. The appearance of lemons packed in different packaging materials (CS/SeNPs, CS/AgNPs, SA/SeNPs and SA/AgNPs) up to 20 days of storage at 5-8 °C. AgNPs: silver nanoparticles, SeNPs: selenium nanoparticles, CS: chitosan, SA: sodium alginate.

CONCLUSION

In this study, a biodegradable active food packaging material was created by combining film-forming substrates (CS or SA) with biosynthesized SeNPs or AgNPs by the reducing agents in the cell-free filtrate of *Aspergillus ochraceus* NSRN22. Compared to the other samples, CS/SeNPs exhibited the highest thermal stability, as evidenced by their lowest mass loss rate. In addition, the mechanical properties of the CS/SeNPs films were better, but the antifungal activity of the CS/AgNPs films was the best against *Penicillium citrinum*. lemons covered with CS/SeNPs for 12 days in the fridge showed no change in color, texture, or physicochemical properties, and the mold growth was significantly decreased. The films made of CS/SeNPs showed the lowest rate of weight loss. The fresh lemons' preservation effect and shelf life were both enhanced by the CS/SeNPs packaging film. In addition, the CS/SeNPs coating that exists could be a great way to supplement with Se micronutrients. The cell viability of films at a concentration of 0.5 mg/mL was 76.7% in CS/SeNPs. This means that the films, when prepared at the concentration of 0.5 mg/mL used in this study, are highly safe for human consumption and use in food. All things considered, the CS/SeNPs films that were made have great potential as components of antimicrobial active packaging, which could keep food safe and extend the shelf life of fruits.

REFERENCES

Abd El-Ghany, MN, Hamdi, SA, Korany, SM, Elbaz, RM, Emam, AN and Farahat, MG. 2023. 'Biogenic silver nanoparticles produced by soil rare actinomycetes and their significant effect on Aspergillus-derived mycotoxins', *Microorganisms*, 11: 1006.

Abd El-Ghany, MN, Yahia, RA and Fahmy, HA. 2023. 'Nanosensors for Agriculture, Water, Environment, and Health.' in, *Handbook of Nanosensors: Materials and Technological Applications* (Springer).

Alizadeh-Sani, M, Ehsani, A, Kia, EM and Khezerlou, A. 2019. 'Microbial gums: Introducing a novel functional component of edible coatings and packaging', *Applied microbiology and biotechnology*, 103: 6853-66.

Alizadeh-Sani, M, Kia, EM, Ghasempour, Z and Ehsani, A. 2021. 'Preparation of active nanocomposite film consisting of sodium caseinate, ZnO nanoparticles and rosemary essential oil for food packaging applications', *Journal of Polymers and the Environment*, 29: 588-98.

Ansari, AQ, Ahmed, SA, Waheed, MA and Juned, S. 2013. 'Extraction and determination of antioxidant activity of Withania somnifera Dunal', *Eur J Exp Biol*, 3: 502-07.

Bagheri, V, Ghanbarzadeh, B, Ayaseh, A, Ostadrahimi, A, Ehsani, A, Alizadeh-Sani, M and Adun, PA. 2019. 'The optimization of physico-mechanical properties of bionanocomposite films based on gluten/carboxymethyl cellulose/cellulose nanofiber using response surface methodology', *Polymer Testing*, 78: 105989.

Baliyan, S, Mukherjee, R, Priyadarshini, A, Vibhuti, A, Gupta, A, Pandey, RP and Chang, C. 2022. 'Determination of antioxidants by DPPH radical scavenging activity and quantitative phytochemical analysis of Ficus religiosa', *Molecules*, 27: 1326.

Carneiro-da-Cunha, MG, Cerqueira, MA, Souza, BWS, Carvalho, S, Quintas, MAC, Teixeira, JA and Vicente, AA. 2010. 'Physical and thermal properties of a chitosan/alginate nanolayered PET film', *Carbohydrate Polymers*, 82: 153-59.

Chen, K, Tian, R, Jiang, J, Xiao, M, Wu, K, Kuang, Y, Deng, P, Zhao, X and Jiang, F. 2024. 'Moisture loss inhibition with biopolymer films for preservation of fruits and vegetables: A review', *International journal of biological macromolecules*: 130337.

Dakhil, AS. 2017. 'Biosynthesis of silver nanoparticle (AgNPs) using Lactobacillus and their effects on oxidative stress biomarkers in rats', *Journal of King Saud University-Science*, 29: 462-67.

Devi, N, Bansal, N, Sharma, S, Dubey, SK and Kumar, S. 2024. 'Novel chitosan-based smart bio-nanocomposite films incorporating TiO2 nanoparticles for white bread preservation', *International journal of biological macromolecules*: 131367.

Dong, W, Su, J, Chen, Y, Xu, D, Cheng, L, Mao, L, Gao, Y and Yuan, F. 2022. 'Characterization and antioxidant properties of chitosan film incorporated with modified silica nanoparticles as an active food packaging', *Food Chemistry*, 373: 131414.

Durán, N, Durán, M, De Jesus, MB, Seabra, AB, Fávaro, WJ and Nakazato, G. 2016. 'Silver nanoparticles: A new view on mechanistic aspects on antimicrobial activity', *Nanomedicine: Nanotechnology, Biology and Medicine*, 12: 789-99.

Ediyilyam, S, George, B, Shankar, SS, Dennis, TT, Wacławek, S, Černík, M and Padil, VV. 2021. 'Chitosan/gelatin/silver nanoparticles composites films for biodegradable food packaging applications', *Polymers*, 13: 1680.

El-Saadony, MT, Saad, AM, Najjar, AA, Alzahrani, SO, Alkhatib, FM, Shafi, ME, Selem, E, Desoky, EM, Fouda, SEE and El-Tahan, AM. 2021. 'The use of biological selenium nanoparticles to suppress Triticum aestivum L. crown and root rot diseases induced by Fusarium

species and improve yield under drought and heat stress', *Saudi journal of biological sciences*, 28: 4461-71.

El-Sayyad, GS, El-Bastawisy, HS, Gobara, M and El-Batal, AI. 2020. 'Gentamicin-assisted mycogenic selenium nanoparticles synthesized under gamma irradiation for robust reluctance of resistant urinary tract infection-causing pathogens', *Biological trace element research*, 195: 323-42.

El Refai, HA, Mohamed, SAI, Aboul Naser, AF, Saleh, AM, Gomaa, SK, Zaki, RA and Hamed, MA. 2024. 'Biogenic synthesized SeONPs by Bacillus paramycoides as antimicrobial, anticancer, antioxidant, apoptotic and hepatorenal treating agent', *Biocatalysis and Agricultural Biotechnology*: 103080.

Elamawi, RM, Al-Harbi, RE and Hendi, AA. 2018. 'Biosynthesis and characterization of silver nanoparticles using Trichoderma longibrachiatum and their effect on phytopathogenic fungi', *Egyptian journal of biological pest control*, 28: 1-11.

Fath-Alla, AA, Khalil, NM, Mohamed, AS and Abd El-Ghany, MN. 2024. 'Antiradical and anti-inflammatory activity of Saccharomyces cerevisiae-mediated selenium nanoparticles', *Egyptian Journal of Botany*, 64: 773-87.

Flórez, M, Guerra-Rodríguez, E, Cazón, P and Vázquez, M. 2022. 'Chitosan for food packaging: Recent advances in active and intelligent films', *Food Hydrocolloids*, 124: 107328.

Gajbhiye, M, Kesharwani, J, Ingle, A, Gade, A and Rai, M. 2009. 'Fungus-mediated synthesis of silver nanoparticles and their activity against pathogenic fungi in combination with fluconazole', *Nanomedicine: Nanotechnology, Biology and Medicine*, 5: 382-86.

Ghaseminezhad, SM, Hamedi, S and Shojaosadati, SA. 2012. 'Green synthesis of silver nanoparticles by a novel method: Comparative study of their properties', *Carbohydrate Polymers*, 89: 467-72.

Gheorghita, R, Gutt, G and Amariei, S. 2020. 'The use of edible films based on sodium alginate in meat product packaging: An eco-friendly alternative to conventional plastic materials', *Coatings*, 10: 166.

Gopinath, V and Velusamy, P. 2013. 'Extracellular biosynthesis of silver nanoparticles using Bacillus sp. GP-23 and evaluation of their antifungal activity towards Fusarium oxysporum', *Spectrochimica Acta Part A: Molecular and Biomolecular Spectroscopy*, 106: 170-74.

Griffin, DH. 1994. 'Spore dormancy and germination', *Fungal physiology*, 2: 375-98.

Gudimalla, A, Jose, J, Rajendran, JV, Gurram, G and Thomas, S. 2022. 'Synthesis of silver nanoparticles by plant extract, incorporated into alginate films and their characterizations', *Chemical Papers*: 1-13.

Heydari, R, Bavandi, S and Javadian, SR. 2015. 'Effect of sodium alginate coating enriched with horsemint (M entha longifolia) essential oil on the quality of bighead carp fillets during storage at 4 C', *Food science & nutrition*, 3: 188-94.

Hu, F, Sun, T, Xie, J, Xue, B, Li, X, Gan, J, Li, L, Bian, X and Shao, Z. 2021. 'Functional properties of chitosan films with conjugated or incorporated salicylic acid', *Journal of Molecular Structure*, 1223: 129237.

Hurtado, A, Aljabali, AAA, Mishra, V, Tambuwala, MM and Serrano-Aroca, Á. 2022. 'Alginate: Enhancement strategies for advanced applications', *International journal of molecular sciences*, 23: 4486.

Ilium, L. 1998. 'Chitosan and its use as a pharmaceutical excipient', *Pharmaceutical research*, 15: 1326-31.

Jain, N, Bhargava, A, Majumdar, S, Tarafdar, JC and Panwar, J. 2011. 'Extracellular biosynthesis and characterization of silver nanoparticles using Aspergillus flavus NJP08: a mechanism perspective', *Nanoscale*, 3: 635-41.

Johnson, LF, Curl, EA, Bond, JH and Fribourg, HA. 1959. 'Methods for studying soil microflora-plant disease relationships'.

Kale, G, Kijchavengkul, T, Auras, R, Rubino, M, Selke, SE and Singh SP. 2007. 'Compostability of bioplastic packaging materials: an overview', *Macromolecular bioscience*, 7: 255-77.

Kanikireddy, V, Kanny, K, Padma, Y, Velchuri, R, Ravi, G, Reddy, BJM and Vithal, M. 2019. 'Development of alginate-gum acacia-Ag0 nanocomposites via green process for inactivation of foodborne bacteria and impact on shelf life of black grapes (Vitis vinifera)', *Journal of Applied Polymer Science*, 136: 47331.

Khalil, NM, Abd El-Ghany, MN and Rodríguez-Couto, S. 2019. 'Antifungal and anti-mycotoxin efficacy of biogenic silver nanoparticles produced by Fusarium chlamydosporum and Penicillium chrysogenum at non-cytotoxic doses', *Chemosphere*, 218: 477-86.

Kulig, D, Zimoch-Korzycka, A, Jarmoluk, A and Marycz, K. 2016. 'Study on alginate–chitosan complex formed with different polymers ratio', *Polymers*, 8: 167.

Lazcano-Ramírez, Gerardo, H, Garza-García, JJ, Hernández-Díaz, JA, León-Morales, JM, Macías-Sandoval, AS and García-Morales, S. 2023. 'Antifungal activity of selenium nanoparticles obtained by plant-mediated synthesis', *Antibiotics*, 12: 115.

Li, C, Wang, K, Li, F and Xie, D. 2024. 'Green fabrication, characterization and antimicrobial activities of AgO/Ag/carboxymethyl chitosan-graphene oxide films', *Arabian Journal of Chemistry*, 17: 105380.

Li, H, Li, W, Zhang, J, Xie, G, Xiong, T and Xu, H. 2022. 'Preparation and characterization of sodium alginate/gelatin/Ag nanocomposite antibacterial film

and its application in the preservation of tangerine', *Food Packaging and Shelf Life*, 33: 100928.

Li, Y, Ying, Y, Zhou, Y, Ge, Y, Yuan, C, Wu, C and Hu, Y. 2019. 'A pH-indicating intelligent packaging composed of chitosan-purple potato extractions strength by surface-deacetylated chitin nanofibers', *International journal of biological macromolecules*, 127: 376-84.

Lin, ZH and Wang, CRC. 2005. 'Evidence on the size-dependent absorption spectral evolution of selenium nanoparticles', *Materials Chemistry and Physics*, 92: 591-94.

Luo, Y and Wang, Q. 2013. 'Recent advances of chitosan and its derivatives for novel applications in food science', *Journal of Food Processing & Beverages*, 1: 1-13.

Luo, Y, Pan, X, Ling, Y, Wang, X and Sun, R. 2014. 'Facile fabrication of chitosan active film with xylan via direct immersion', *Cellulose*, 21: 1873-83.

Mohammed, AE, Korany, SM, Sonbol, H, Alhomaidi, EA, Alwakeel, SS and Elbaz, RM. 2024. 'Myco-fabricated silver nanoparticle by novel soil fungi from Saudi Arabian desert and antimicrobial mechanism', *Scientific reports*, 14: 15211.

Nair, MS, Tomar, M, Punia, S, Kukula-Koch, W and Kumar, M. 2020. 'Enhancing the functionality of chitosan-and alginate-based active edible coatings/films for the preservation of fruits and vegetables: A review', *International journal of biological macromolecules*, 164: 304-20.

Nikzamir, M, Akbarzadeh, A and Panahi, Y. 2021. 'An overview on nanoparticles used in biomedicine and their cytotoxicity', *Journal of Drug Delivery Science and Technology*, 61: 102316.

Nunes, MR, Castilho, MdSM, Veeck, APdL, da Rosa, CG, Noronha, CM, Maciel, MV and Barreto, PM. 2018. 'Antioxidant and antimicrobial methylcellulose films containing Lippia alba extract and silver nanoparticles', *Carbohydrate Polymers*, 192: 37-43.

Perera, KY, Sharma, S, Duffy, B, Pathania, S, Jaiswal, AK and Jaiswal, S. 2022. 'An active biodegradable layer-by-layer film based on chitosan-alginate-TiO2 for the enhanced shelf life of tomatoes', *Food Packaging and Shelf Life*, 34: 100971.

Priyadarshini, S, Gopinath, V, Priyadharsshini, NM, MubarakAli, D and Velusamy, P. 2013. 'Synthesis of anisotropic silver nanoparticles using novel strain, Bacillus flexus and its biomedical application', *Colloids and surfaces B: Biointerfaces*, 102: 232-37.

Qiao, ZP, Wang, MY, Liu, JF and Wang, QZ. 2022. 'Green synthesis of silver nanoparticles using a novel endophytic fungus Letendraea sp. WZ07: Characterization and evaluation of antioxidant, antibacterial and catalytic activities (3-in-1 system)', *Inorganic Chemistry Communications*, 138: 109301.

Qin, Y, Liu, Y, Yuan, L, Yong, H and Liu, J. 2019. 'Preparation and characterization of antioxidant, antimicrobial and pH-sensitive films based on chitosan, silver nanoparticles and purple corn extract', *Food Hydrocolloids*, 96: 102-11.

Rayman, MP. 2012. 'Selenium and human health', *The Lancet*, 379: 1256-68.

Riseh, RS, Vatankhah, M, Hassanisaadi, M, Shafiei-Hematabad, Z and Kennedy, JF. 2023. 'Advancements in coating technologies: unveiling the potential of chitosan for the preservation of fruits and vegetables', *International journal of biological macromolecules*: 127677.

Safaei, M, Taran, M, and Imani, MM. 2019. 'Preparation, structural characterization, thermal properties and antifungal activity of alginate-CuO bionanocomposite', *Materials Science and Engineering: C*, 101: 323-29.

Salem, SS, Fouda, MMG, Fouda, A, Awad, MA, Al-Olayan, EM, Allam, AA and Shaheen, TI. 2021. 'Antibacterial, cytotoxicity and larvicidal activity of green synthesized selenium nanoparticles using Penicillium corylophilum', *Journal of Cluster Science*, 32: 351-61.

Schulz, H and Baranska, M. 2007. 'Identification and quantification of valuable plant substances by IR and Raman spectroscopy', *Vibrational Spectroscopy*, 43: 13-25.

Shaheen, TI, Salem, SS and Fouda, A. 2021. 'Current advances in fungal nanobiotechnology: Mycofabrication and applications', *Microbial nanobiotechnology: Principles and applications*: 113-43.

Shankar, S, Jaiswal, L, Aparna, RSL, Prasad, RGSV, Kumar, GP and Manohara, CM. 2015. 'Wound healing potential of green synthesized silver nanoparticles prepared from Lansium domesticum fruit peel extract', *Materials Express*, 5: 159-64.

Shankar, S, Wang, LF and Rhim, JW. 2016. 'Preparations and characterization of alginate/silver composite films: Effect of types of silver particles', *Carbohydrate Polymers*, 146: 208-16.

Shehata, SA, Abdelrahman, SZ, Megahed, MMA, Abdeldaym, EA, El-Mogy, MM and Abdelgawad, KF. 2021. 'Extending shelf life and maintaining quality of tomato fruit by calcium chloride, hydrogen peroxide, chitosan, and ozonated water', *Horticulturae*, 7: 309.

Shiekh, KA, Ngiwngam, K and Tongdeesoontorn, W. 2021. 'Polysaccharide-based active coatings incorporated with bioactive compounds for reducing postharvest losses of fresh fruits', *Coatings*, 12: 8.

Soares, JdP, Santos, JE, Chierice, GO and Cavalheiro, ETG. 2004. 'Thermal behavior of alginic acid and its sodium salt', *Eclética Química*, 29: 57-64.

Soltani, Z, Tavakolipour, H and Tabari, M. 2023. 'The influence of chitosan and titanium dioxide

nanoparticles incorporated with polylactic acid on prolonging rye bread shelf life', *Journal of Food Measurement and Characterization*, 17: 1806-16.

Srivastava, N and Mukhopadhyay, M. 2015. 'Green synthesis and structural characterization of selenium nanoparticles and assessment of their antimicrobial property', *Bioprocess and biosystems engineering*, 38: 1723-30.

Suresh, AK, Pelletier, DA, Wang, W, Broich, ML, Moon, JW, Gu, B, Allison, DP, Joy, DC, Phelps, TJ and Doktycz, MJ. 2011. 'Biofabrication of discrete spherical gold nanoparticles using the metal-reducing bacterium Shewanella oneidensis', *Acta biomaterialia*, 7: 2148-52.

Tang, S, Gao, X, Guo, H, Guan, Y, Lin, M and Zheng, Z. 2023. 'Effects of silver nanoparticle/graphene oxide composite on the properties of polymethyl methacrylate base material in vitro', *Materials Technology*, 38: 2214025.

Tran, TH, Le, XC, Tran, TNM, Nguyen, NTT, Pham, BN and Vu, D. 2023. 'Nano selenium–alginate edible coating extends hydroponic strawberry shelf life and provides selenium fortification as a micro-nutrient', *Food Bioscience*, 53: 102597.

Wahab, YA, Al-Ani, LA, Khalil, I, Schmidt, S, Tran, NN, Escribà-Gelonch, M, Woo, MW, Davey, K, Gras, S and Hessel, V. 2024. 'Nanomaterials: A critical review of impact on food quality control and packaging', *Food control*: 110466.

Wang, H, Zhang, J and Yu, H. 2007. 'Elemental selenium at nano size possesses lower toxicity without compromising the fundamental effect on selenoenzymes: comparison with selenomethionine in mice', *Free Radical Biology and Medicine*, 42: 1524-33.

Xing, Y, Wang, X, Guo, X, Yang, P, Yu, J, Shui, Y, Chen, C, Li, X, Xu, Q and Xu, L. 2021. 'Comparison of antimicrobial activity of chitosan nanoparticles against bacteria and fungi', *Coatings*, 11: 769.

Xu, LP, Han, D, Wu, X, Zhang, Q, Zhang, X and Wang, S. 2016. 'A green route for substrate-independent oil-repellent coatings', *Scientific reports*, 6: 38016.

Xu, L, Cao, W, Li, R, Zhang, H, Xia, N, Li, T, Liu, X and Zhao, X. 2019. 'Properties of soy protein isolate/nano-silica films and their applications in the preservation of Flammulina velutipes', *Journal of Food Processing and Preservation*, 43: e14177.

Zhang, H, Zhou, H, Bai, J, Li, Y, Yang, J, Ma, Q and Qu, Y. 2019. 'Biosynthesis of selenium nanoparticles mediated by fungus Mariannaea sp. HJ and their characterization', *Colloids and Surfaces A: Physicochemical and Engineering Aspects*, 571: 9-16.